OPTIMIZATION OF HEAT TRANSFER ENHANCEMENT IN PLANE COUETTE FLOW

Shingo Motoki, Genta Kawahara and Masaki Shimizu
Graduate School of Engineering Science
Osaka University
1-3 Machikaneyama, Toyonaka, Osaka 560-8531, Japan
motoki@tes.me.es.osaka-u.ac.jp

ABSTRACT

We have theoretically explored a velocity field optimizing heat transfer in plane Couette flow. The velocity field is supposed to be incompressible, time-independent and periodic in the wall-parallel directions, and temperature is determined in terms of the velocity as a solution to an advection-diffusion equation. The Prandtl number is set to unity, and the consistent boundary conditions are imposed on the velocity and temperature fields. The excess of a wall heat flux (or equivalently total scalar dissipation) over total energy dissipation is taken as an objective functional. By using a variational method, the Euler–Lagrange equations are derived, and numerically solved to find the optimal states in the sense of maximization of the functional.

At small Reynolds number $Re \sim 10^1$, the optimal state exhibits a two-dimensional velocity field which consists of streamwise-independent large-scale circulation rolls. They play a role in heat transfer enhancement with respect to the conductive state as in thermal convection. At higher Reynolds number $Re \gtrsim 10^2$, however, a three-dimensional optimal state arises from symmetry breaking of the two-dimensional state. The three-dimensional velocity field consists of the large-scale rolls and smaller-scale hierarchical quasi-streamwise tube-like vortices near the walls. The streamwise vortex tubes are tilted in the spanwise direction so that they may produce the vorticity antiparallel to the mean-shear vorticity. The significant three-dimensionality leads to optimal heat transfer enhancement, and much higher wall heat flux is achieved with less energy dissipation than those of a turbulent state.

1 INTRODUCTION

Turbulence has an ability of significantly high heat transfer in comparison with laminar flow, but it results in an increase in friction loss as a consequence of simultaneous promotion of momentum transfer. This is well known as the similarity between heat and momentum transfer in engineering (Reynolds, 1874; Chilton & Colburn, 1934), and it suggests difficulty in simultaneous achievement of heat transfer enhancement and skin friction reduction. Especially, for fluids with the Prandtl number, the ratio between thermal and momentum diffusivity, is close to unity (e.g. about 0.7 for air), the heat and momentum transfer shows strong similarity (Dipprey & Sabersky, 1963). If innovative flow control techniques to break the similarity and to maximize the dissimilarity are developed, it will lead to dramatic improvement of the performance of heat exchangers. Recently, by applying an active feedback control to heat transfer in wall-bounded turbulent flow with blowing and suction on the wall, Hasegawa & Kasagi (2011) and Yamamoto *et al.* (2013) have numerically achieved the dissimilarity enhancement even when the Prandtl number is equal to unity. In the near future, the accomplishment of flow control for dissimilar heat transfer enhancement might be expected.

The aim of this study is to find an optimal velocity field which serves as a target of such flow controls. For thermal convection, a lot of studies have been made on velocity field leading to maximal transport (in other words, maximal mixing) for over 60 years (Malkus, 1954; Howard, 1963). Recently, Hassanzadeh *et al.* (2014) have reported optimal transport under the two types of constraints (fixed kinematic energy or fixed enstrophy) in two-dimensional thermal convection. On the other hand, Sondak *et al.* (2015) have obtained solutions to the steady Navier–Stokes equation based on Oberbeck–Boussinesq approximation, which achieve maximal heat transfer in the two-dimensional domain. However, three-dimensional optimal states or optimal heat transfer enhancement in shear flows have not been discussed as yet.

We focus on heat transfer in plane Couette flow, and define an objective functional as the excess of the total scalar dissipation (or equivalently, a total wall heat flux) over the total energy dissipation. Using a variational method, we derive the Euler–Lagrange equations which determine an optimal state. The present paper reports characteristics of the optimal state obtained as a solution to the Euler–Lagrange equations and a significant effect on heat transfer enhancement of three-dimensional tube-like vortex structures observed in the optimal velocity field.

2 FORMULATION

Figure 1 shows the configuration of the velocity and temperature fields. The flow is driven by the parallel plates moving in the opposite directions at a constant speed. The upper (or lower) wall surface is held at higher (or lower) constant temperature. The coordinates, x, y and z are used for the representation of the streamwise, the wall-normal and the spanwise directions, respectively, and their origin is on the midplane of the channel. The corresponding components of the velocity $\underline{u}(x,y,z)$ are given by u, v and w in the streamwise, the wall-normal and the spanwise directions,

respectively.

Let us consider heat transfer in an incompressible time-independent velocity field fulfilling the continuity equation

$$\underline{\nabla}\cdot\underline{u}=0. \tag{1}$$

We suppose that the temperature field $T(x,y,z)$ is determined as a solution to an advection-diffusion equation

$$\underline{u}\cdot\underline{\nabla}T=\kappa\underline{\nabla}^2T, \tag{2}$$

where κ denotes a thermal diffusivity. The velocity and temperature fields are supposed to be periodic in the streamwise (x-) and the spanwise (z-) directions. The boundary conditions

$$\underline{u}(x,\pm h,z)=\pm U\underline{e}_x,\quad T(x,\pm h,z)=\pm T_0 \tag{3}$$

are imposed on the walls, where $\underline{e}_x$ is the unit vector in the x-direction.

We decompose the temperature into a conduction part and a fluctuation about it as

$$T=T_0\frac{y}{h}+\theta. \tag{4}$$

Taking a volume average of the product of equation (2) with θ and taking into account the boundary condition (3), we have the expression of the wall heat flux as

$$-\kappa\frac{\mathrm{d}\overline{T}}{\mathrm{d}y}(+h)=-\kappa\frac{\mathrm{d}\overline{T}}{\mathrm{d}y}(-h)=-\frac{\kappa h}{T_0}\left\langle|\underline{\nabla}\theta|^2\right\rangle-\kappa\frac{T_0}{h}, \tag{5}$$

where $\overline{(\cdot)}$ and $\langle\cdot\rangle$ denote the average over wall-parallel planes and the volume average, respectively. The first term in the right hand side of equation (5) is referred to as "scalar dissipation".

On the other hand, the steady motion of a viscous fluid is described by the Navier–Stokes equation

$$\underline{u}\cdot\underline{\nabla}\,\underline{u}=-\frac{1}{\rho}\underline{\nabla}p+\nu\underline{\nabla}^2\underline{u}+\underline{f}, \tag{6}$$

where p is the pressure, ρ and ν are the mass density and the kinematic viscosity of the fluid, respectively. $\underline{f}$ is external body force per unit mass. The volume average of the inner product of equation (6) with the velocity $\underline{u}$ and the boundary condition (3) yield the expression of the wall momentum flux as

$$\frac{\nu}{2}\left[\frac{\mathrm{d}\overline{u}}{\mathrm{d}y}(+h)+\frac{\mathrm{d}\overline{u}}{\mathrm{d}y}(-h)\right]=\frac{\nu h}{U}\left\langle|\underline{\nabla}\,\underline{u}|^2\right\rangle-\frac{h}{U}\left\langle\underline{u}\cdot\underline{f}\right\rangle, \tag{7}$$

where the first and second terms in the right-hand side represent energy dissipation and energy input by the external force, respectively.

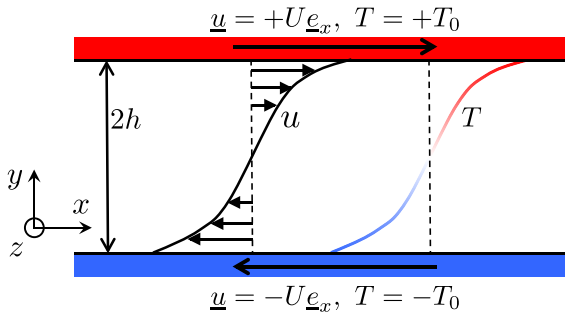

Figure 1. Configuration of the velocity and temperature fields.

As can be seen from equation (5) and (7), the wall heat flux corresponds to the scalar dissipation, and the wall momentum flux (i.e. the skin friction) is related with the energy dissipation. To find an optimal state for the dissimilarity between momentum and heat transfer, we introduce the dimensionless objective functional $J_\star$ as

$$J_\star=\left\langle\frac{\lambda}{2RePr}|\underline{\nabla}_\star\theta_\star|^2-\frac{1}{2Re}|\underline{\nabla}_\star\,\underline{u}_\star|^2\right.$$
$$\left.+p^*_\star(\underline{\nabla}_\star\cdot\underline{u}_\star)+\lambda\theta^*_\star\left(\underline{u}_\star\cdot\underline{\nabla}_\star\theta_\star+v_\star-\frac{1}{RePr}\underline{\nabla}^2_\star\theta_\star\right)\right\rangle. \tag{8}$$

Each dimensionless quantity is normalized as

$$x_\star=\frac{x}{h},\ J_\star=\frac{J}{U^3/h},$$
$$\theta_\star=\frac{\theta}{T_0},\ \theta^*_\star=\frac{\theta^*}{T_0},\ \underline{u}_\star=\frac{\underline{u}}{U},\ p^*_\star=\frac{p^*}{\rho U^2}, \tag{9}$$

where $\star$ represents a dimensionless quantity. λ is the dimensionless weight of the contribution from the heat transfer against the momentum transfer. $Re=Uh/\nu$ and $Pr=\nu/\kappa$ are the Reynolds number and the Prandtl number, respectively. $p^*_\star(x_\star,y_\star,z_\star)$ and $\theta^*_\star(x_\star,y_\star,z_\star)$ are Lagrange multipliers subject to the constraints (1) and (2). We suppose that $\theta^*_\star$ satisfies the boundary conditions on the walls, $\theta^*_\star(x_\star,\pm1,z_\star)=0$. The first variation of the functional $J_\star$ and the Euler–Lagrange equations are respectively written as

$$\delta J_\star=\left\langle\frac{\delta J_\star}{\delta\underline{u}_\star}\cdot\delta\underline{u}_\star+\frac{\delta J_\star}{\delta\theta_\star}\delta\theta_\star+\frac{\delta J_\star}{\delta\theta^*_\star}\delta\theta^*_\star+\frac{\delta J_\star}{\delta p^*_\star}\delta p^*_\star\right\rangle \tag{10}$$

and

$$\frac{\delta J_\star}{\delta\underline{u}_\star}\equiv-\underline{\nabla}_\star p^*_\star+\frac{1}{Re}\underline{\nabla}^2_\star\underline{u}_\star+\lambda\theta^*_\star\underline{\nabla}_\star\theta_\star+\lambda\theta^*_\star\underline{e}_y=\underline{0} \tag{11}$$
$$\frac{\delta J_\star}{\delta\theta_\star}\equiv\underline{u}_\star\cdot\underline{\nabla}_\star\theta^*_\star+\frac{1}{RePr}\underline{\nabla}^2_\star\theta^*_\star+\frac{1}{RePr}\underline{\nabla}^2_\star\theta_\star=0 \tag{12}$$
$$\frac{\delta J_\star}{\delta\theta^*_\star}\equiv\underline{u}_\star\cdot\underline{\nabla}_\star\theta_\star-\frac{1}{RePr}\underline{\nabla}^2_\star\theta_\star+v_\star=0 \tag{13}$$
$$\frac{\delta J_\star}{\delta p^*_\star}\equiv\underline{\nabla}_\star\cdot\underline{u}_\star=0, \tag{14}$$

where $\underline{e}_y$ is the unit vector in the $y_\star$-direction. By solving the equations (11)-(14) using a spectral-Galerkin Newton-

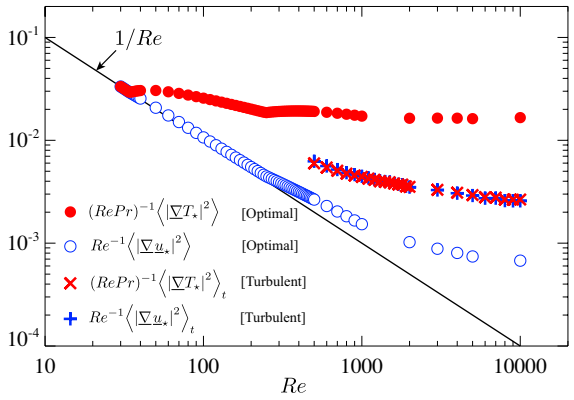

Figure 2. Total scalar dissipation and total energy dissipation as a function of Re in the optimal and turbulent state for $Pr = 1$ and $\lambda = 0.1$.

GMRES method, we seek a velocity field which gives a maximal point of $J_\star$.

3 RESULTS AND DISCUSSION

3.1 Characteristics of optimal states

Figure 2 shows the total scalar dissipation and the total energy dissipation in the optimal state obtained for the Prandtl number $Pr = 1$ and the weight coefficient $\lambda = 0.1$. The time-averaged dissipation of the plane turbulent Couette flow is also plotted for comparison purposes. $\langle\cdot\rangle_t$ denotes averaging over the volume and time. The solid line represents the value in the laminar flow, $1/Re$, which provides the lower bound of the total scalar and energy dissipation. At quite small Reynolds number $Re < 35$, the laminar conductive field is an optimal state. At higher Re, however, the optimal state exhibits two-dimensional velocity field as shown in figure 3(a). Figure 3 shows the flow structures and temperature fields in the optimal states. The red (or blue) isosurfaces represent the positive (or negative) streamwise vorticity in the lower half of the channel, and the contours show cross-stream velocity fields and temperature fields in the plane $x/h = 2\pi(= 0)$. The two-dimensional optimal state shown in figure 3(a) consists of streamwise-independent large-scale circulation rolls that play a role in heat transfer from the upper wall to the lower wall. In turbulent flow, the scalar and energy dissipation take almost the same value due to the similarity between momentum and heat transfer. For the optimal state at large Re, meanwhile, the much higher scalar dissipation (i.e., much higher wall heat flux) is achieved with the less energy dissipation than those of the turbulent flow. As shown in figure 3(b) and 3(c) , the optimal states exhibit three-dimensional velocity fields. In the velocity field, there appear smaller-scale quasi-streamwise tube-like vortices near the walls in addition to the large-scale circulation rolls with the width of half the spanwise period $L_z/h = \pi$. The wall-normal component of the velocity is dominant in the central region of the channel. Small-scale vortices are observed only in the near-wall regions. They produce high temperature gradient to enhance local heat transfer, by pushing the hotter (or colder) fluid onto the lower (or upper) wall. As Re increases, smaller and stronger quasi-streamwise vortices appear near the walls.

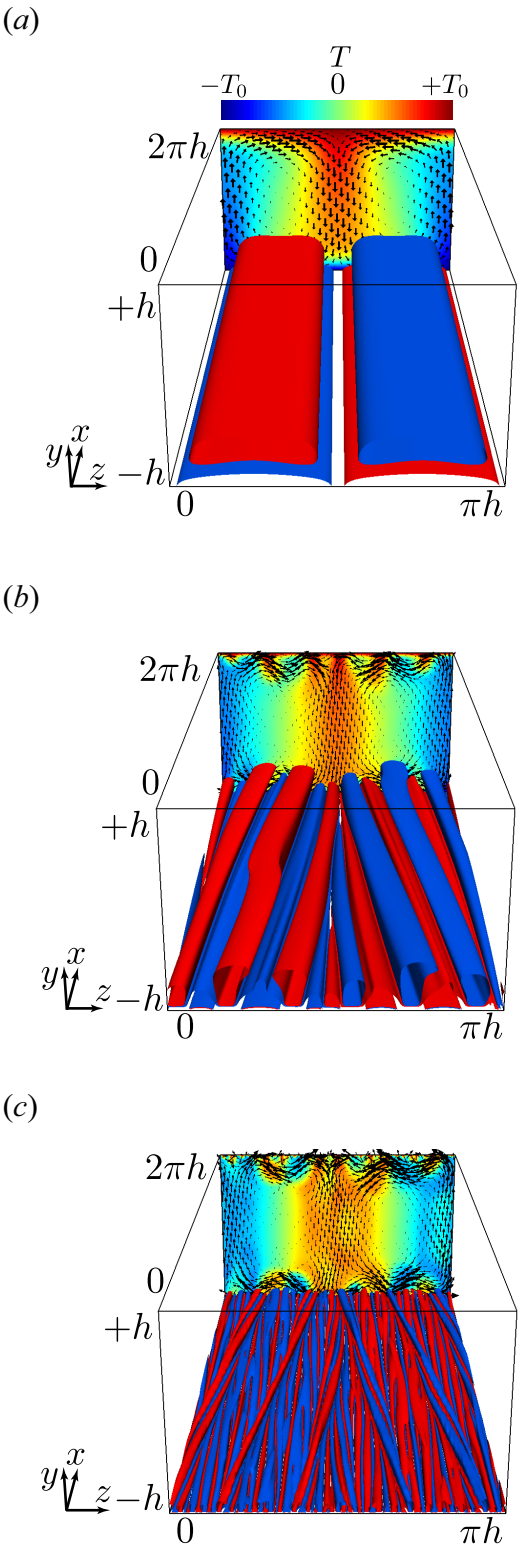

Figure 3. Isosurfaces of the streamwise vorticity in the optimal state at (a) $Re = 200$, (b) $Re = 1000$ and (c) $Re = 5000$ for $Pr = 1$ and $\lambda = 0.1$. Only those in the lower half of the channel ($y < 0$) are shown for visualization of the structures near the lower wall. Red objects represent an isosurface of the streamwise vorticity (a) $\omega_x/(U/h) = +0.3$, (b) $\omega_x/(U/h) = +0.5$ and (c) $\omega_x/(U/h) = +2.0$. Blue objects represent an isosurface of (a) $\omega_x/(U/h) = -0.3$, (b) $\omega_x/(U/h) = -0.5$ and (c) $\omega_x/(U/h) = -2.0$. The contours and the vectors represent temperature field T and velocity field (w, v) in the plane $x/h = 2\pi(= 0)$.

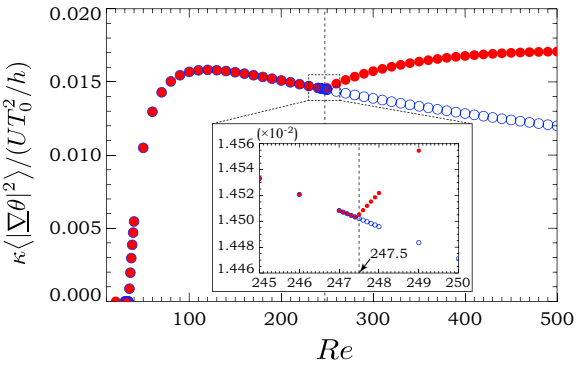

Figure 4. Scalar dissipation as a function of Re for $Pr = 1$ and $\lambda = 0.1$. Red filled circles denote the scalar dissipation in the optimal state and blue open circles stand for that obtained from the optimization only within a streamwise-independent two-dimensional velocity field.

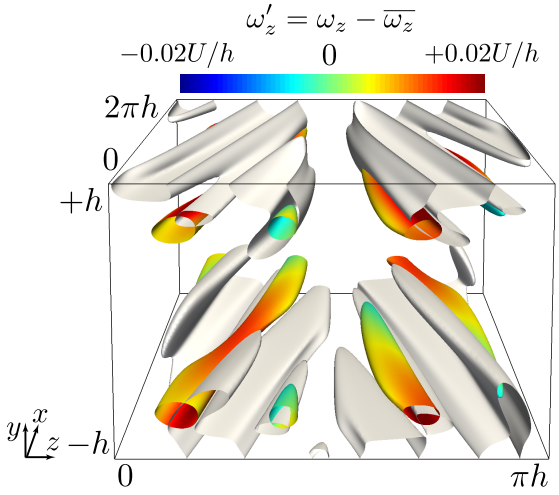

Figure 5. Vortical structures and significant increases in the local scalar dissipation for the optimal velocity field against the two-dimensional optimal velocity field at $Re = 249$ for $Pr = 1$ and $\lambda = 0.1$. The colored objects represent isosurfaces, $Q = +0.03U^2/h^2$, of the second invariant of velocity gradient tensor, on which the distribution of the spanwise vorticity fluctuation $\omega_z' = \omega_z - \overline{\omega_z}$ is shown. The white objects indicate isosurfaces of an increase in the local scalar dissipation, $D_S - D_S^{2D} = +0.001(UT_0^2/h)$.

3.2 Effects of flow three-dimensionality on local scalar dissipation

Figure 4 shows the scalar dissipation in the optimal state at small Re. The blue open circles represent optimal state obtained by the optimization in a streamwise-independent two-dimensional velocity field. The two-dimensional optimal solution emerges from supercritical pitchfork bifurcation on the laminar solution at $Re = 35$. As Re increases further, the secondary pitchfork bifurcation occurs on the two-dimensional solution branch at $Re = 247.5$ to create a three-dimensional optimal solution which gives higher scalar dissipation. Figure 5 visualizes isosurfaces of a positive value of the second invariant of the velocity gradient tensor

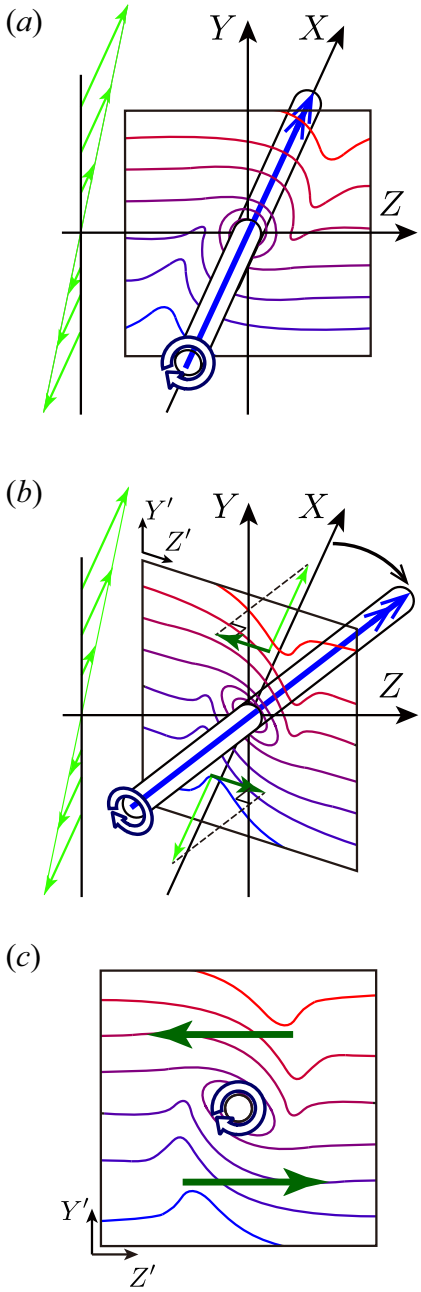

Figure 6. Illustration of scalar fields around vortex tubes in shear flow. (a,b) Configuration of the vortex tube in the shear flow. In (b), the vortex tube is inclined from the X-axis on the plane $Y = 0$. (c) Isocontours of the scalar in the (Z', Y')-plane normal to the central axis of the vortex tube.

$$Q = -\frac{\partial u_i}{\partial x_j}\frac{\partial u_j}{\partial x_i} \tag{15}$$

in the optimal state at $Re = 249$. The isosurfaces are colored by the spanwise vorticity fluctuation $\omega_z' = \omega_z - \overline{\omega_z}$ on the Q isosurface. Most parts of the extracted tube-like vortex structures indicate $\omega_z' > 0$, and this result implies that the vortex tubes are tilted in the spanwise direction so that they may produce the spanwise vorticity antiparallel to the vor-

ticity of the shear flow produced by the moving walls. The white isosurface shows the region with significant increase of the local scalar dissipation from the two-dimensional solution at the same value of Re. The local scalar dissipation defined as

$$D_S = \kappa \left(\frac{\partial T}{\partial x_j} \right)^2 . \tag{16}$$

Note that the volume average of D_S is consistent with the total scalar dissipation. It can be seen that the regions of $D_S - D_S^{2D} > 0$ distribute around the vortices, where the superscript 2D means the two-dimensional solution. The mechanism of the local heat transfer enhancement can be explained by using the simple model shown in figure 6. The illustrations show the scalar field around a vortex tube in shear flow. The isocontours indicate the scalar field in the plane normal to the central axis of the vortex tube. As shown in these figures, the vortex tube spirally wraps the isosurfaces of the scalar around itself through the convective transfer induced by swirling flow. When the direction of the central axis of the vortex tube is consistent with that of the X-axis (figure 6a), the shear flow has no effect on the scalar field because it is tangent to the scalar isosurfaces everywhere. Now we consider that the vortex tube is inclined from the X-axis on the plane $Y = 0$, so that it may produce the vorticity antiparallel to that of the shear flow (figure 6b). We refer to the tilted vortex as anticyclonic vortex. As shown in figure 6(c), the vortex tighten the spacing of the wrapped isocontours of the scalar around itself. It turns out that the scalar dissipation (i.e., heat flux) is locally intensified in the flanks of the anticyclonic vortex, which have been observed in the optimal state (figure 5).

3.3 Hierarchical structure in optimal state

Figure 7 shows the spanwise energy spectra of the wall-normal velocity as a function of the distance from the wall $y+h$ and the spanwise wavelength l at $Re = 1000$-5000. In figure 7(a), $y+h$ and l are non-dimensionalized by half the channel width h. The peaks at $(l/h, y/h+1) = (\pi, 1)$ indicate the large-scale circulation rolls, and they are observed at any Re. On the other hand, a lot of peaks are observed along the 'ridge' represented by the dashed line $l = \pi(y+h)$, that is the near-wall quasi-streamwise vortex tubes in the optimal states possess hierarchical self similarity. The length scale of the largest vortices scales with the outer length h, and their height is $y/h+1 \approx 0.2$ regardless of Re. Here, we introduce the inner length δ_T which characterises the near-wall temperature profile as

$$\delta_T = T_0 \left(\frac{\mathrm{d}\overline{T}}{\mathrm{d}y}(+h) \right)^{-1} = T_0 \left(\frac{\mathrm{d}\overline{T}}{\mathrm{d}y}(-h) \right)^{-1} . \tag{17}$$

In figure 7(b), $y+h$ and l are normalized by δ_T. It can be seen that the spectral density distribution scales with the inner length δ_T in vicinity to the wall. The self-similar vortex structures exist in the range of $\delta_T \lesssim y+h \lesssim 0.2h$ at any Re.

Shown in figure 8 is the mean temperature profile in the optimal state at $Re = 1000-5000$. As Re increases, the profile in the central region of the channel is more flattened, while the gradient at the wall is steeper. Figures 9 and 10 respectively show the mean temperature and the mean heat flux profiles as a function of the distance

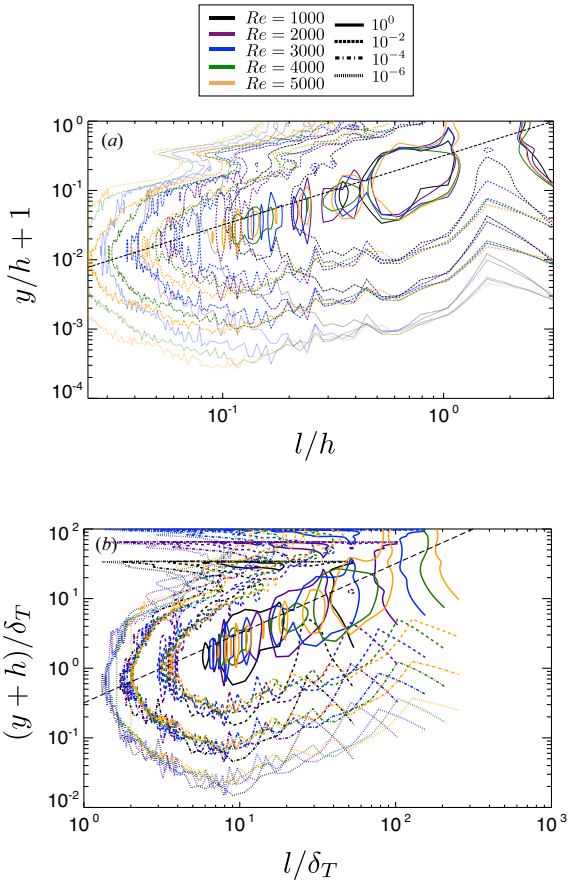

Figure 7. Spanwise energy spectra of the wall-normal velocity as a function of the distance from the wall $y+h$ and the spanwise wavelength l in the optimal state for $Pr = 1$ and $\lambda = 0.1$. The distance from the wall $y+h$ and the wavelength l are normalized by (a) half the channel width h and (b) the inner length δ_T. The diagonal lines show $l = \pi(y+h)$.

to the wall, $(y+h)/\delta_T$. At $(y+h)/\delta_T \ll 1$, the profile corresponds to $\overline{T}/T_0 + 1 = (y+h)/\delta_T$, since the diffusion dominants over the advection. In the intermediate region $1 \lesssim (y+h)/\delta_T \lesssim 10$ where the hierarchical vortex structures exist, the logarithmic-like profile can be observed. The dashed line represents the logarithmic fit determined in the range $1 < (y+h)/\delta_T < 10$, $\overline{T}/T_0 + 1 = 0.086 \ln((y+h)/\delta_T) + 0.81$. It is well known that a logarithmic mean velocity profile appears in near-wall turbulence where self-similar hierarchical vortical structures are commonly observed. As can be seen from the similarity between momentum and heat transfer, heat transfer in the turbulent flow also shows the logarithmic mean temperature profile. On the other hand, in recent years, the logarithmic temperature distribution has also been found in thermal convection turbulence (Ahlers *et al.*, 2012, 2014). To clarify the effect of the hierarchical self-similar vortex structures on optimal heat transfer at large Reynolds numbers and to reveal that correspondence relation between such structures and the logarithmic profile are left for future study.

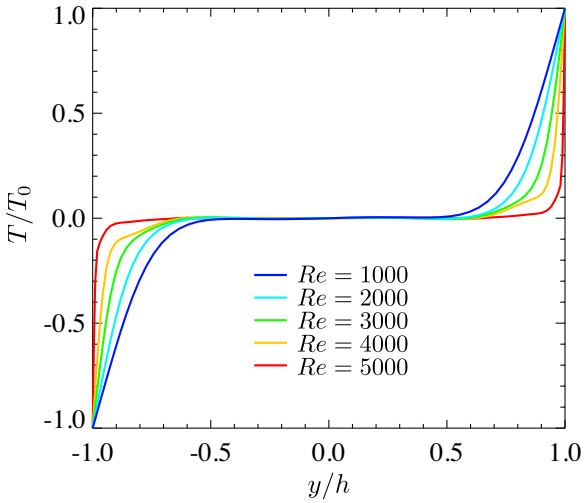

Figure 8. Mean temperature profiles in the optimal states for $Pr = 1$ and $\lambda = 0.1$.

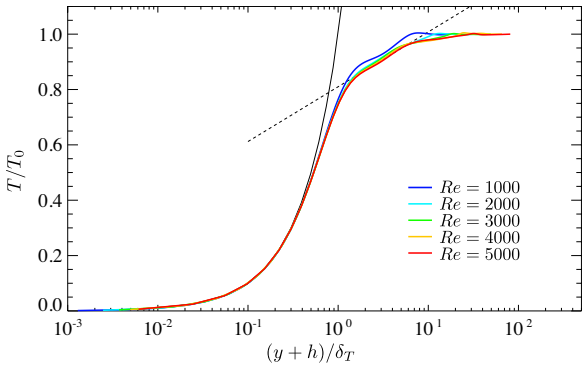

Figure 9. Mean temperature profiles as a function of the distance to the wall $y+h$ normalized by the inner length δ_T in the optimal states for $Pr = 1$ and $\lambda = 0.1$. The solid curve indicates $\overline{T}/T_0 + 1 = (y+h)/\delta_T$, and the dashed line shows the logarithmic fit $\overline{T}/T_{T_0} + 1 = 0.086 \ln[(y+h)/\delta_T] + 0.81$ determined in the range $1 < (y+h)/\delta_T < 10$.

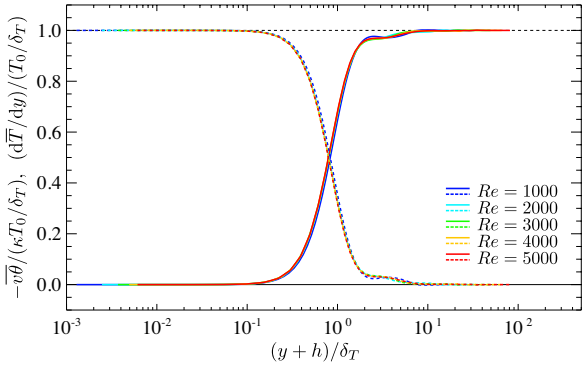

Figure 10. Convective and conductive heat fluxes as a function of the distance to the wall $y+h$ normalized by the inner length δ_T in the optimal states for $Pr = 1$ and $\lambda = 0.1$. The solid and dashed curves represent the convective heat fluxes $-\overline{v\theta}$ and the conductive heat fluxes $\mathrm{d}\overline{T}/\mathrm{d}y$ normalized by the inner length, respectively.

REFERENCES

Ahlers, G., Bodenschatz, E., Funfschilling, D., Grossmann, S., He, X., Lohse, D., R.Stevens & Verzicco, R. 2012 Logarithmic temperature profiles in turbulent Rayleigh–Bénard convection. *Phys. Rev. Lett.* **109** (114501).

Ahlers, G., Bodenschatz, E. & He, X. 2014 Logarithmic temperature profiles of turbulent Rayleigh–Bénard convection in the classical and ultimate state for a Prandtl number of 0.8. *J. Fluid Mech.* **758**, 436–467.

Chilton, T. H. & Colburn, A. P. 1934 Mass transfer (absorption) coefficients prediction from data on heat transfer and fluid friction. *Ind. Eng. Chem.* **26**, 1183–1187.

Dipprey, D. F. & Sabersky, R. H. 1963 Heat and momentum transfer in smooth and rough tubes at various Prandtl numbers. *J. Heat and Mass Transfer* **6**, 329–353.

Hasegawa, Y. & Kasagi, N. 2011 Dissimilar control of momentum and heat transfer in a fully developed turbulent channel flow. *J. Fluid Mech.* **683**, 57–93.

Hassanzadeh, P., Chini, G. P. & Doering, C. R. 2014 Wall to wall optimal transport. *J. Fluid Mech.* **751**, 627–662.

Howard, L. N. 1963 Heat transport by turbulent convection. *J. Fluid Mech.* **17**, 405–432.

Malkus, W. V. R. 1954 The heat transport and spectrum of thermal turbulence. *Proc. R. Soc. Lond.* A **225**, 196–212.

Reynolds, O. 1874 On the extent and action of the heating surface of steam boilers. *Proc. Lit. Phil. Soc. Manchester* **14**, 7–12.

Sondak, D., Smith, L. M. & Waleffe, F. 2015 Optimal heat transport solutions for Rayleigh–Bénard convection. *J. Fluid Mech.* **784**, 565–595.

Yamamoto, A., Hasegawa, Y. & Kasagi, N. 2013 Optimal control of dissimilar heat and momentum transfer in a fully developed turbulent channel flow. *J. Fluid Mech.* **733**, 189–220.